Freeze-thaw decellularization of the trabecular meshwork in an ex vivo eye perfusion model

Yalong Dang[1], Susannah Waxman[1], Chao Wang[1, 2], Adrianna Jensen[1], Ralitsa Loewen[1], Richard Bilonick[1], Nils Loewen[1]

Affiliations:

1: Department of Ophthalmology, School of Medicine, University of Pittsburgh, Pittsburgh, United States of America

2: Department of Ophthalmology, Xiangya School of Medicine, Central South University, Changsha, China

* Corresponding author:
Nils A. Loewen, MD, PhD
203 Lothrop St
Suite 819
Pittsburgh, PA 15213
Email: Loewen.nils@gmail.com
Phone: 412-944-2554

Abstract

Objective: Trabecular meshwork (TM) is the primary substrate of outflow resistance in glaucomatous eyes. Repopulating diseased TM with fresh, functional TM cells might represent a novel therapeutic breakthrough. Various decellularized TM scaffolds were developed by ablating existing cells with suicide gene therapy or saponin, but always with incomplete cell removal or dissolve the extracellular matrix. We hypothesized that a chemical-free, freeze-thaw method would be able to produce a fully decellularized TM scaffold for cell transplantation.

Materials and Methods: We obtained 24 porcine eyes from a local abattoir, dissected and mounted them in an anterior segment perfusion and pressure transduction system within two hours of sacrifice. After they stabilized for 72 hours, eight eyes each were assigned to freeze-thaw (F) ablation (-80°C×2), to 0.02% saponin (S) treatment, or the control group (C), respectively. The trabecular meshwork was transduced with an eGFP expressing feline immunodeficiency viral (FIV) vector and tracked via fluorescent microscopy to confirm ablation. Following treatment, the eyes were perfused with standard tissue culture medium for 180 hours. We assessed histological changes by hematoxylin and eosin staining. TM cell viability was evaluated with a calcein AM/propidium iodide (PI) assay. We measured IOP and modeled it with a linear mixed effects model using a B-spline function of time with 5 degrees of freedom.

Results: F and and S experienced a similar IOP reduction by 30% from baseline (P=0.64). IOP reduction occurred of about 30% occurred in F within 24 hours and in S within 48 hours. Live visualization of eGFP demonstrated that F conferred a complete ablation of all TM cells and only a partial ablation in S. Histological analysis confirmed that no TM cells survived in F while the excellular matrix remained. The viability assay showed very low PI and no calcein staining in F in contrast to numerous PI-labeled dead TM cells and calcein-labeled viable TM cells in S.

Conclusion: We developed a rapid TM ablation method that uses cyclic freezing that is free of biological or chemical agents and able to produce produce a decellularized TM scaffold with preserved TM excellular matrix in an organotypic perfusion culture.

PeerJ Preprints | https://doi.org/10.7287/peerj.preprints.2736v1 | CC BY 4.0 Open Access | rec: 18 Jan 2017, publ: 18 Jan 2017

Introduction

The trabecular meshwork (TM) is the primary substrate of outflow resistance in normal and glaucomatous eyes. Recent studies suggested not only low TM cellularity (Alvarado, Murphy & Juster, 1984; Baleriola et al., 2008), but also TM cytoskeletal changes and phagocytosis changes in primary open angle glaucoma (Clark et al., 1995; Fatma et al., 2009; Izzotti et al., 2010; Saccà, Pulliero & Izzotti, 2015; Peters et al., 2015; Micera et al., 2016). Repopulating diseased TM with fresh, functional TM cells has been shown to to restore homeostasis of normal outflow and thus might represent a novel therapeutic breakthrough (Du et al., 2013; Abu-Hassan et al., 2015; Yun et al., 2016; Zhu et al., 2016).

For TM cell transplantation studies, it appears that both an extracellular architecture similar to that of native TM and a low TM cellularity as seen in POAG patients are valuable for distinct purposes. In a recent study, an ex vivo 3D bioengineered TM scaffold repopulated by human primary TM cells was developed, but it failed to mimic the three-layered structure of human TM (Torrejon et al., 2016). In vivo, mouse glaucoma models induced by photocoagulation of episcleral vein or transgenic technique (such as Tg-MYOC ^{Y437H}) were used for TM transplantation (Yun et al., 2014; Zhu et al., 2016). However, the anatomy of the rodent outflow tract is distinguished from that of humans in that rodent models house 3-4 TM cell layers and a discontinuous Schlemm's canal (Chen, Zhao & Zhang, 2016). Porcine eyes have more similarities with human eyes in terms of size, structure, intraocular pressure (IOP), and the outflow pattern (Sanchez et al., 2011; Loewen et al., 2016b,a). Recently, porcine anterior segment treated with saponin was used to create decellularized TM scaffold for cell transplantation (Abu-Hassan et al., 2015). As a result, 36%±9% of total TM cells were ablated after 10 minutes of saponin treatment.

Although saponin supplemented media was subsequently replaced with standard serum-free TM perfusion medium, the impact of saponin on the metabolism of remaining and transplanted TM cells as well as the ECM is difficult to determine.

To address these concerns, a chemical-free, freeze-thaw method was developed to produce a decellularized TM scaffold. Together with our anterior segment perfusion system (Loewen et al., 2016b), this ex vivo porcine TM scaffold for cell transplantation can provide framework for real-time TM visualization and IOP measurement.

PeerJ Preprints | https://doi.org/10.7287/peerj.preprints.2736v1 | CC BY 4.0 Open Access | rec: 18 Jan 2017, publ: 18 Jan 2017

Materials and Methods

Study Design

Pig eyes were obtained from a local abattoir and prepared for culture within 2 hours of death. Twenty-four eyes were assigned to three groups with eight eyes in each to serve as controls, undergo free-thaw cycles or be infused with saponin. This number was chosen based on past power calculations and the maximum number that could be perfused simultaneously thereby minimizing the variability with same group experiments with our setup (Loewen et al., 2016b,a). Anterior segment perfusion cultures were allowed to stabilize for 72 hours before subject to freeze thaw cycles or saponin supplemented media, respectively. The intraocular pressure (IOP) was recorded continuously by a pressure transducer system (Physiological Pressure Transducer, SP844; MEMSCAP, Skoppum, Norway) (Loewen et al., 2016b,a). Eyes cultures were continued for another 180 hours. Two additional eyes per ablation method group were transduced with eGFP expressing feline immunodeficiency viral vectors and subjected to the same ablation methods as used in the experimental groups. Expression of eGFP was monitored and compared. Two eyes per group were randomly selected for viability assays and histological analysis.

Preparation of Porcine Anterior Segments and Perfusion System

After removing extraocular tissues, freshly enucleated porcine eyes from a local abattoir (Thoma Meat Market, Saxonburg, PA) were placed into a into 5% povidone-iodine solution (NC9771653, Fisher Scientific, Waltham, MA) for 3 minutes and rinsed three times with phosphate-buffered saline (PBS). Eyes were hemisected 7 mm posterior and parallel to the limbus and the lens, ciliary body, and iris were carefully removed. Anterior segments were again washed with PBS three times and mounted in anterior segment perfusion dishes. Media (phenol-free DMEM (SH30284, HyClone, GE Healthcare, UK)) supplemented with 1% fetal bovine serum and 1% antibiotic-antimycotic (15240062, Thermo Fisher Scientific, Waltham, MA) was continuously pumped into the anterior chambers at a constant infusion rate of 3 microliters per minute. After calibration, the IOP was recorded in 2 minute intervals.

Trabecular Ablation by Freeze-Thaw cycles or 0.02% Saponin

After 72 hours of allowing eyes to stabilize, eyes were subjected to freeze-thaw cycles or 0.02% saponin, respectively. For the freeze-thaw ablation, anterior segments were exposed to -80°C for 2 hours, then thawed at room temperature for 1 hour. After two cycles of freeze-thaw, anterior segments were reconnected to the perfusion system. For the saponin ablation, the regular perfusion media was replaced with 0.02% saponin supplemented media for 15 minutes, then exchanged for the normal perfusion medium in 37 °C incubator as described before (Abu-Hassan et al., 2015).

Anterior Segment Transduction and TM Visualization

Feline immunodeficiency viral vectors expressing eGFP were generated by transient cotransfection of envelope plasmid pMD.G, packaging plasmid pFP93, and gene-transfer plasmid encoding eGFP and neomycin resistance GINSIN (Saenz et al., 2007; Oatts et al., 2013; Zhang et al., 2014) using a polyethylenimine method (Loewen et al., 2016b). Vector containing supernatant from transfected 293T cells were harvested two, four and six days after transfection and concentrated by

ultracentrifugation. 10^7 transducing units (TU) of GINSIN were injected into the anterior chambers. eGFP expression was followed through the bottom of the culture dish using a dissecting microscope equipped for epifluorescence (SZX16, Olympus, Tokyo, Japan).

TM Viability Analysis and Histology

TM cell viability was assessed by calcein acetoxymethyl (calcein AM) and propidium iodide (PI) co-labelling (Gonzalez, Hamm-Alvarez & Tan, 2013). After 180 hours, the anterior segments were collected and washed with PBS three times. The limbus with the TM was dissected and incubated with calcein AM (0.3 µM, C1430, Thermo Fisher, Waltham, MA) and PI (1 µg/ml, P1304MP, Thermo Fisher, Waltham, MA) for 30 min at 37°C. After three additional PBS washes, the TM was flat-mounted, and imaged under an upright laser scanning confocal microscope at 400-fold magnification (BX61, Olympus, Tokyo, Japan). Images were captured at three distinct TM depths corresponding to the three meshwork layers, the innermost, uveoscleral, corneoscleral and cribriform TM closest to Schlemm's canal. TM samples obtained from at least two separate quadrants per eye were dissected and fixed with 4% paraformaldehyde in PBS for 24 hours. After rinsing them three times in PBS, they were embedded in paraffin, sectioned at 6 micron thickness and stained with hematoxylin and eosin.

Statistics

Data were presented as mean ± standard error and analyzed by PASW 18.0 (SPSS Inc., Chicago, IL, USA). One-way ANOVA was performed for the comparison of IOP and TM cellularity among the different groups. Statistical difference was considered significant if $p<0.05$. A linear mixed effects model was fitted to the fold change response in R (Core Team, 2016). The response was modeled as a B-spline function of time with 5 degrees of freedom (Berk; Hu et al., 1998).

PeerJ Preprints | https://doi.org/10.7287/peerj.preprints.2736v1 | CC BY 4.0 Open Access | rec: 18 Jan 2017, publ: 18 Jan 2017

Results

Gross morphology and histology

Two eyes per group were discarded due to leaks while the baseline was established. In eyes that were successfully cultured, the gross morphology of the anterior chamber remained well preserved after two freeze-thaw cycles, with light opacification of the cornea as the most notable change (**Fig. 1**). Histology from within 24 hours after exposure to freeze-thaw (F) or saponin (S) indicated that F preserved the microarchitecture better **(Fig. 2 A and B)** than S **(Fig. 2 C)**. Blue stained nucleoli could still be observed but disappeared later consistent with the viability assay results described below. There was less extracellular matrix material present in S than in C and F.

Monitoring of TM ablation

Ablation control eyes were transduced with 1×10^7 eGFP FIV vectors prior to F and S. 24 hours after transduction, the TM cells began to express eGFP, reaching a peak intensity at 48 hours, as reported previously (Loewen et al., 2016b; Dang et al., 2016b). There were discontinuous areas of transduced TM (**Fig. 3 top**) and transduction along corneal stretch folds as well as sclera. Two cycles of -80°C completely abolished eGFP expression. Two cycles were necessary because pilot eyes with only one cycle still showed some eGFP positive cells. In contrast, after 0.02% saponin perfusion, eGFP fluorescence appeared quenched and only a small portion of transduced cells was ablated 24 hours after exposure (**Fig. 3 bottom**).

Trabecular meshwork viability assay

After two weeks of perfusion, most cells in all three TM layers from the negative control group were labeled by Calcein AM (**Fig. 5a-Fig. 5c**), while only occasional cells were stained with PI (**Fig. 5b and Fig. 5c**). In contrast, no Calcein AM staining and very few PI stained cells were found in the freeze-thaw group (**Fig. 5d-Fig. 5f**). Different from the above two groups, most of the TM cells in S were labeled by PI, with few cells in the uveal and corneoscleral TM demonstrating a light calcein AM staining (**Fig. 5g-Fig. 5h**).

Intraocular pressure

A stable baseline was established for all anterior segments for 72 hours prior to F or S. IOP varied insignificantly by 10.3±7.5 % throughout the end of the study (*Ps*>0.05 compared to the baseline) **(Fig. 5)**. However, pressure decreased dramatically after either freeze-thaw or saponin (baseline freeze-thaw 14.75±2.24 mmHg, saponin 14.37± 1.14 mmHg, *P*=0.288). At 12 hours, F dropped to 70% ±7.1% and S to 79.2±8.1% of baseline, respectively. F remained significantly lower than C for 96 hours (p= 0.02) but eye experienced a larger IOP variability onward resulting in reduced significance. In contrast, S had a significantly lower IOP throughout the study until the experimental endpoint at 180 hours. We applied a linear mixed effects model that used a B-spline function of time with 5 degrees of freedom (Berk) **(Fig. 6)**. The results reflect the the averages shown in Fig. 5 and confirm the three non-linear behaviors with distinctly different patterns. F had an intercept, representative of the initial IOP drop, that was -0.378 fold less (p<0.001) than C and a standard error of 0.088 with 15 degrees of freedom and a t-value of -4.3. F was not significantly different from S in the B-spline function model (p=0.142). S had an intercept that

PeerJ Preprints | https://doi.org/10.7287/peerj.preprints.2736v1 | CC BY 4.0 Open Access | rec: 18 Jan 2017, publ: 18 Jan 2017

was 0.242 fold less than C (p=0.013) with a standard error of 0.086, 15 degrees of freedom and a t-value of -2.8.

Discussion

In this study, we developed a method to decellularize the trabecular meshwork in anterior segment perfusion cultures quickly and reliably. This was achieved with two cycles of freezing at -80°C and thawing at room temperature. This avoids use of chemical agents that might dissolve the extracellular matrix or have other, not yet discovered effects. We compared this method to saponin mediated disruption. Each methods has distinct properties and advantages:

Freeze-thaw cycles, applied here to group F, have been used extensively before to ablate tissues as a treatment of human diseases (Erinjeri & Clark, 2010; Baust et al., 2014; Chu & Dupuy, 2014) including cyclocryodestruction in glaucoma (Benson & Nelson, 1990). It has also been used in research (Baust et al., 2014; Chan & Ooi, 2016; Liu et al., 2016) and in food production ("Fish and Fishery Products Hazards and Controls Guidance"; Gill, 2006; Craig, 2012). Mechanisms of cryoablation in medicine include direct cell injury, vascular injury, ischemia, apoptosis, and immunomodulation (Chu & Dupuy, 2014): cell injury during freezing causes dehydration from the so called solution effect that causes the earlier freezing extracellular compartment to extract solutes, an osmotic gradient and cell shrinkage (Lovelock, 1953) that can be enhanced by ice crystal formation within the cell, damaging organelles and the cell membrane. During thawing, the intracellular compartment shifts to hypertonia, attracting fluid that causes the cell to burst. Mechanisms not at work in our model presented here are direct cold-induced coagulative necrosis that is the result from sublethal temperatures that activate apoptosis (Baust & Gage, 2005) and direct, cold-induced coagulative necrosis from vascular injury as a result of stasis, thrombosis and ischemia. An interesting clinical effect is the intense immunogenicity after cryoablation that is different from heat coagulation as immunogenic epitopes are preserved (Jansen et al., 2010).

Saponin, used in experimental group S, can be used to destroy cells through lysis. At lower concentrations, it has been used to reduce viability of cells (Abu-Hassan et al., 2015). It is an enormously large class of chemical compounds that exists in a range of plant species (Saponaria) which has the ability to produce soap-like foam when shaken in aqueous solution and has been used in early soaps (Coombes, 2012). These substances are amphiphilic (both hydro- and lipophilic) glycosides in which a sugar is bound to a functional three-terpene group via a glycosidic bond. Saponins are an important subset of saponins that are steroidal while aglycone derivatives have pharmacologic characteristics of alkaloids. Historically, saponins have been used as a fish poison for fishing (Campbell, 1999). In research and treatment, their ability to form complexes with cholesterol to create pores in cell membrane bilayers to induce lysis or enhance penetration of macromolecules, has been used (Holmes et al., 2015). These properties may have wide-ranging and difficult to characterize effects in cell transplantation models. Each purchased batch may have a different composition of compounds which may make it necessary to characterize features and concentrations for different lots and could reduce the reproducibility of experiments.

PeerJ Preprints | https://doi.org/10.7287/peerj.preprints.2736v1 | CC BY 4.0 Open Access | rec: 18 Jan 2017, publ: 18 Jan 2017

The macroscopic appearance had only relatively minor changes in F and S and included a mild opacification of the cornea. The microscopic architecture was best preserved in F but less so in S. This can be expected based on the properties of these two different methods described above. Especially the change of permeability of cell membranes by saponin can cause worsened edema by allowing fluids to enter the extracellular space more easily compared to freeze-thaw that is more likely to cause dehydration. Compared to the cells themselves, many blue nuclei persisted in early histology because they are less permeable and contain less fluids compared to the cytoplasm. These observations were reflected in the ablation of transduced, eGFP expressing cells. Freeze-thaw caused nearly complete loss of fluorescence after the first cycle and disappeared entirely when cells were disrupted after the second cycle. Saponin appears to have caused leakage of eGFP proteins where diminished fluorescence was observed but only few cells were fully lysed.

The viability cell confirms our findings from the histological analysis and eGFP ablation. Freeze-thaw caused disappearance of almost all cells secondary to the above mechanism of cell dehydration and subsequent burst. Saponin appears to have been a sublethal injury to many cells, especially in the uveal and corneoscleral TM. Abu-Hassan et al have optimized a protocol to induce a sublethal injury with saponin that is able to mimic glaucoma in an ex vivo model in which the glaucoma phenotype could be treated successfully (Abu-Hassan et al., 2015). This also matches the slower decline seen in a model of inducible cytoablation mediated by an HSVtk suicide vector (Zhang et al., 2014).

This pattern of cell death matches the IOP reduction of groups F and S. F experienced a more immediate drop compared to S as could be expected by a more complete breakdown of the outflow regulation by the TM. In comparison, the slower downslope seen after saponin exposure likely reflects the more gradual cell function decline with eventual cell death. The eventual IOP was lower in S which may represent the loss not only of cells but also of extracellular matrix which could persist in eyes in F to a variable extent and time. Our use of a b-spline function of time provides for the first time function modeling for a biological system of effects in an eye culture model that play out over a period of time rather than the common comparison of single time points which assumes that observations from one time point to the other are largely unrelated (Hu et al., 1998). Handling longitudinal data this way allows for an extension of the standard linear mixed-effects models that can arround for a wide range of non-linear behaviours. They are robust to small sample sizes, as well as to noisy observations and missing data.

Consistent with our clinical (Dang et al., 2016c,a) and laboratory findings (Zhang et al., 2014), TM ablation resulted in the reduction of IOP. A (20.80 ± 8.05)% IOP reduction was achieved at 12 hours after saponin treatment, while a greater (30.00 ± 7.13)% IOP reduction was achieved in the freeze-thaw group. The freeze-thaw cycle removed all the meshwork cells, including corneoscleral and cribriform meshwork cells which account for at least 50% of trabecular outflow resistance, whereas most of these cells were preserved after saponin ablation. It is possible that the IOP reduction seen after cyclocryodestruction is partially due to an improvement of conventional outflow, not just of reduced aqueous humor production or uveoscleral outflow enhancement from inflammation.

PeerJ Preprints | https://doi.org/10.7287/peerj.preprints.2736v1 | CC BY 4.0 Open Access | rec: 18 Jan 2017, publ: 18 Jan 2017

Limitations of this study are that cytoablation via freeze thaw may liberate other, undesirable factors from non-trabecular cells that also die. The argument against a profound impact of those is that the macroscopic and microscopic structures were surprisingly stable for the entire time of 10 days. We only describe an ablation method here but not a repopulation of the trabecular meshwork by cell transplantation.

In conclusion, we developed a fast, inexpensive and reliable method that results in complete ablation of TM cells while the architecture including trabecular beams were well-preserved.

Funding

NEI K08-EY022737

The Initiative to Cure Glaucoma of the Eye and Ear Foundation of Pittsburgh

Reference

Abu-Hassan DW., Li X., Ryan EI., Acott TS., Kelley MJ. 2015. Induced Pluripotent Stem Cells Restore Function in a Human Cell Loss Model of Open-Angle Glaucoma. *Stem cells* 33:751–761.

Alvarado J., Murphy C., Juster R. 1984. Trabecular meshwork cellularity in primary open-angle glaucoma and nonglaucomatous normals. *Ophthalmology* 91:564–579.

Baleriola J., García-Feijoo J., Martínez-de-la-Casa JM., Fernández-Cruz A., de la Rosa EJ., Fernández-Durango R. 2008. Apoptosis in the trabecular meshwork of glaucomatous patients. *Molecular vision* 14:1513–1516.

Baust JG., Gage AA. 2005. The molecular basis of cryosurgery. *BJU international* 95:1187–1191.

Baust JG., Gage AA., Bjerklund Johansen TE., Baust JM. 2014. Mechanisms of cryoablation: clinical consequences on malignant tumors. *Cryobiology* 68:1–11.

Benson MT., Nelson ME. 1990. Cyclocryotherapy: review of cases over 10-year. *The British journal of ophthalmology* 74:103–105.

Berk M. Smoothing-splines Mixed-effects Models in R using the sme Package: a Tutorial.

Campbell PD. 1999. *Survival Skills of Native California*. Gibbs Smith.

Chan JY., Ooi EH. 2016. Sensitivity of thermophysiological models of cryoablation to the thermal and biophysical properties of tissues. *Cryobiology* 73:304–315.

Chen L., Zhao Y., Zhang H. 2016. Comparative Anatomy of the Trabecular Meshwork, the Optic Nerve Head and the Inner Retina in Rodent and Primate Models Used for Glaucoma Research. *Vision research* 1:4.

Chu KF., Dupuy DE. 2014. Thermal ablation of tumours: biological mechanisms and advances in therapy. *Nature reviews. Cancer* 14:199–208.

Clark AF., Miggans ST., Wilson K., Browder S., McCartney MD. 1995. Cytoskeletal changes in cultured human glaucoma trabecular meshwork cells. *Journal of glaucoma* 4:183–188.

Coombes AJ. 2012. *The A to Z of Plant Names: A Quick Reference Guide to 4000 Garden Plants*. Timber Press.

Core Team R. 2016. *R: A Language and Environment for Statistical Computing*. Vienna, Austria: R Foundation for Statistical Computing.

Craig N. 2012. Fish tapeworm and sushi. *Canadian family physician Medecin de famille canadien* 58:654–658.

Dang Y., Kaplowitz K., Parikh HA., Roy P., Loewen RT., Francis BA., Loewen NA. 2016a. Steroid-induced glaucoma treated with trabecular ablation in a matched comparison to primary open angle glaucoma. *Clinical & experimental ophthalmology*. DOI: 10.1111/ceo.12796.

Dang Y., Loewen R., Parikh HA., Roy P., Loewen NA. 2016b. Gene transfer to the outflow tract. *Experimental eye research*:044396.

Dang Y., Roy P., Bussel II., Loewen RT., Parikh H., Loewen NA. 2016c. Combined analysis of trabectome and phaco-trabectome outcomes by glaucoma severity. *F1000Research* 5:762.

Du Y., Yun H., Yang E., Schuman JS. 2013. Stem cells from trabecular meshwork home to TM tissue in vivo. *Investigative ophthalmology & visual science* 54:1450–1459.

Erinjeri JP., Clark TWI. 2010. Cryoablation: mechanism of action and devices. *Journal of vascular and interventional radiology: JVIR* 21:S187–91.

Fatma N., Kubo E., Toris CB., Stamer WD., Camras CB., Singh DP. 2009. PRDX6 attenuates oxidative stress- and TGF β -induced abnormalities of human trabecular meshwork cells. *Free radical research* 43:783–795.

Fish and Fishery Products Hazards and Controls Guidance

Gill CO. 2006. Microbiology of Frozen Foods. In: *Handbook of Frozen Food Processing and Packaging*. crcnetbase.com, 85–100.

Gonzalez JM Jr., Hamm-Alvarez S., Tan JCH. 2013. Analyzing live cellularity in the human trabecular meshwork. *Investigative ophthalmology & visual science* 54:1039–1047.

Hitchings RA., Crowston JG., Sherwood MB., Shaarawy TM. 2009. *Glaucoma: Expert Consult Premium Edition - Enhanced Online Features, Print, and DVD, 2-Volume Set*. Elsevier Health Sciences.

Holmes SE., Bachran C., Fuchs H., Weng A., Melzig MF., Flavell SU., Flavell DJ. 2015. Triterpenoid saponin augmention of saporin-based immunotoxin cytotoxicity for human leukaemia and lymphoma cells is partially immunospecific and target molecule dependent. *Immunopharmacology and immunotoxicology* 37:42–55.

Hu FB., Goldberg J., Hedeker D., Flay BR., Pentz MA. 1998. Comparison of Population-Averaged and Subject-Specific Approaches for Analyzing Repeated Binary Outcomes. *American journal of epidemiology* 147:694–703.

Izzotti A., Saccà SC., Longobardi M., Cartiglia C. 2010. Mitochondrial damage in the trabecular meshwork of patients with glaucoma. *Archives of ophthalmology* 128:724–730.

Jansen MC., van Hillegersberg R., Schoots IG., Levi M., Beek JF., Crezee H., van Gulik TM. 2010. Cryoablation induces greater inflammatory and coagulative responses than radiofrequency ablation or laser induced thermotherapy in a rat liver model. *Surgery* 147:686–695.

Kaplowitz K., Loewen NA. 2014. Minimally Invasive Glaucoma Surgery: Trabeculectomy Ab Interno. In: *Surgical Innovations in Glaucoma*. Springer New York, 175–186.

LeCluyse EL., Witek RP., Andersen ME., Powers MJ. 2012. Organotypic liver culture models: meeting current challenges in toxicity testing. *Critical reviews in toxicology* 42:501–548.

Liu X., Zhao G., Shu Z., Niu D., Zhang Z., Zhou P., Cao Y., Gao D. 2016. Quantification of Intracellular Ice Formation and Recrystallization During Freeze-Thaw Cycles and Their Relationship with the Viability of Pig Iliac Endothelium Cells. *Biopreservation and biobanking* 14:511–519.

Loewen RT., Brown EN., Roy P., Schuman JS., Sigal IA., Loewen NA. 2016a. Regionally Discrete Aqueous Humor Outflow Quantification Using Fluorescein Canalograms. *PloS one* 11:e0151754.

Loewen RT., Roy P., Park DB., Jensen A., Scott G., Cohen-Karni D., Fautsch MP., Schuman JS., Loewen NA. 2016b. A Porcine Anterior Segment Perfusion and Transduction Model With Direct Visualization of the Trabecular Meshwork. *Investigative ophthalmology & visual science* 57:1338–1344.

Lovelock JE. 1953. The haemolysis of human red blood-cells by freezing and thawing. *Biochimica et biophysica acta* 10:414–426.

Micera A., Quaranta L., Esposito G., Floriani I., Pocobelli A., Saccà SC., Riva I., Manni G., Oddone F. 2016. Differential Protein Expression Profiles in Glaucomatous Trabecular Meshwork: An Evaluation Study on a Small Primary Open Angle Glaucoma Population. *Advances in therapy* 33:252–267.

Oatts JT., Zhang Z., Tseng H., Shields MB., Sinard JH., Loewen NA. 2013. In vitro and in vivo comparison of two suprachoroidal shunts. *Investigative ophthalmology & visual science* 54:5416–5423.

Oh JW., Hsi T-C., Guerrero-Juarez CF., Ramos R., Plikus MV. 2013. Organotypic skin culture. *The Journal*

of investigative dermatology 133:e14.

Peters JC., Bhattacharya S., Clark AF., Zode GS. 2015. Increased Endoplasmic Reticulum Stress in Human Glaucomatous Trabecular Meshwork Cells and Tissues. *Investigative ophthalmology & visual science* 56:3860–3868.

Philpott MP., Green MR., Kealey T. 1990. Human hair growth in vitro. *Journal of cell science* 97 (Pt 3):463–471.

Rapid learning curve assessment in an ex vivo training system for microincisional glaucoma surgery 2016. DOI: 10.13140/RG.2.2.20962.12482.

Saccà SC., Pulliero A., Izzotti A. 2015. The dysfunction of the trabecular meshwork during glaucoma course. *Journal of cellular physiology* 230:510–525.

Saenz D., Barraza R., Loewen N., Teo W., Kemler I., Poeschla E. 2007. Production and Use of Feline Immunodeficiency Virus (FIV)-Based Lentiviral Vectors. In: Friedmann T, Rossi JJ eds. *Gene Transfer: Delivery and Expression of DNA and RNA : a Laboratory Manual*. CSHL Press, 57–73.

Sanchez I., Martin R., Ussa F., Fernandez-Bueno I. 2011. The parameters of the porcine eyeball. *Graefe's archive for clinical and experimental ophthalmology = Albrecht von Graefes Archiv fur klinische und experimentelle Ophthalmologie* 249:475–482.

Taurone S., Ripandelli G., Pacella E., Bianchi E., Plateroti AM., De Vito S., Plateroti P., Grippaudo FR., Cavallotti C., Artico M. 2015. Potential regulatory molecules in the human trabecular meshwork of patients with glaucoma: immunohistochemical profile of a number of inflammatory cytokines. *Molecular medicine reports* 11:1384–1390.

Torrejon KY., Papke EL., Halman JR., Stolwijk J., Dautriche CN., Bergkvist M., Danias J., Sharfstein ST., Xie Y. 2016. Bioengineered glaucomatous 3D human trabecular meshwork as an in vitro disease model. *Biotechnology and bioengineering* 113:1357–1368.

Vranka JA., Kelley MJ., Acott TS., Keller KE. 2015. Extracellular matrix in the trabecular meshwork: intraocular pressure regulation and dysregulation in glaucoma. *Experimental eye research* 133:112–125.

Yun H., Lathrop KL., Yang E., Sun M., Kagemann L., Fu V., Stolz DB., Schuman JS., Du Y. 2014. A laser-induced mouse model with long-term intraocular pressure elevation. *PloS one* 9:e107446.

Yun H., Zhou Y., Wills A., Du Y. 2016. Stem Cells in the Trabecular Meshwork for Regulating Intraocular Pressure. *Journal of ocular pharmacology and therapeutics: the official journal of the Association for Ocular Pharmacology and Therapeutics* 32:253–260.

Zhang Z., Dhaliwal AS., Tseng H., Kim JD., Schuman JS., Weinreb RN., Loewen NA. 2014. Outflow tract ablation using a conditionally cytotoxic feline immunodeficiency viral vector. *Investigative ophthalmology & visual science* 55:935–940.

Zhang Y-S., Niu L-Z., Zhan K., Li Z-H., Huang Y-G., Yang Y., Chen J-B., Xu K-C. 2016. Percutaneous imaging-guided cryoablation for lung cancer. *Journal of thoracic disease* 8:S705–S709.

Zhu W., Gramlich OW., Laboissonniere L., Jain A., Sheffield VC., Trimarchi JM., Tucker BA., Kuehn MH. 2016. Transplantation of iPSC-derived TM cells rescues glaucoma phenotypes in vivo. *Proceedings of the National Academy of Sciences of the United States of America*. DOI: 10.1073/pnas.1604153113.

Zondervan PJ., Buijs M., de la Rosette JJ., van Delden O., van Lienden K., Laguna MP. 2016. Cryoablation of small kidney tumors. *International journal of surgery* 36:533–540.

PeerJ Preprints | https://doi.org/10.7287/peerj.preprints.2736v2 | CC BY 4.0 Open Access | rec: 18 Jan 2017, publ: 18 Jan 2017

Figures

Figure 1

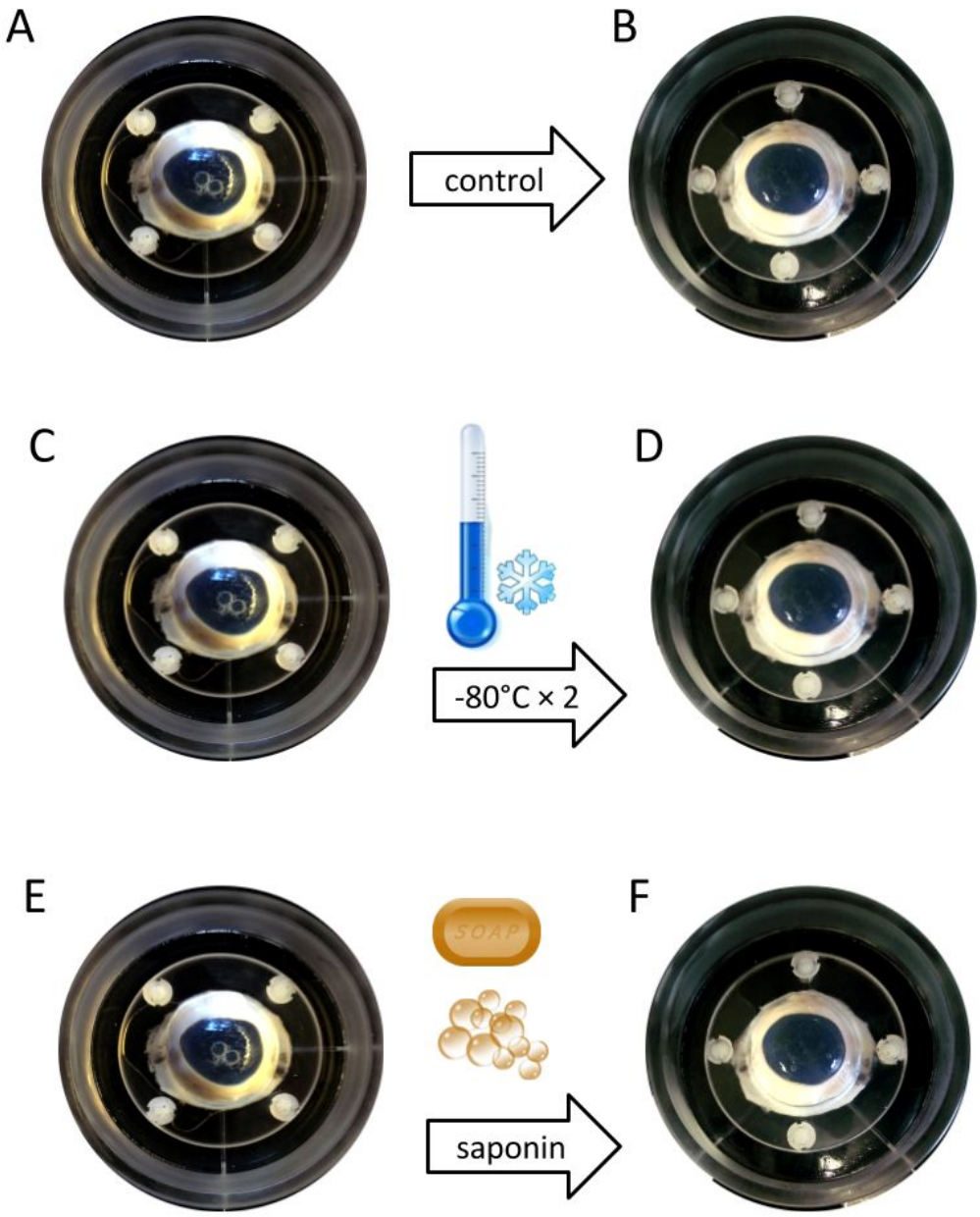

Figure 1: Freeze thaw treatment of anterior segment cultures. Eyes were exposed to two cycles of freezing at -80°C followed by thawing at room temperature. The macroscopic appearance remained mostly unchanged.

PeerJ Preprints | https://doi.org/10.7287/peerj.preprints.2736v1 | CC BY 4.0 Open Access | rec: 18 Jan 2017, publ: 18 Jan 2017

Figure 2

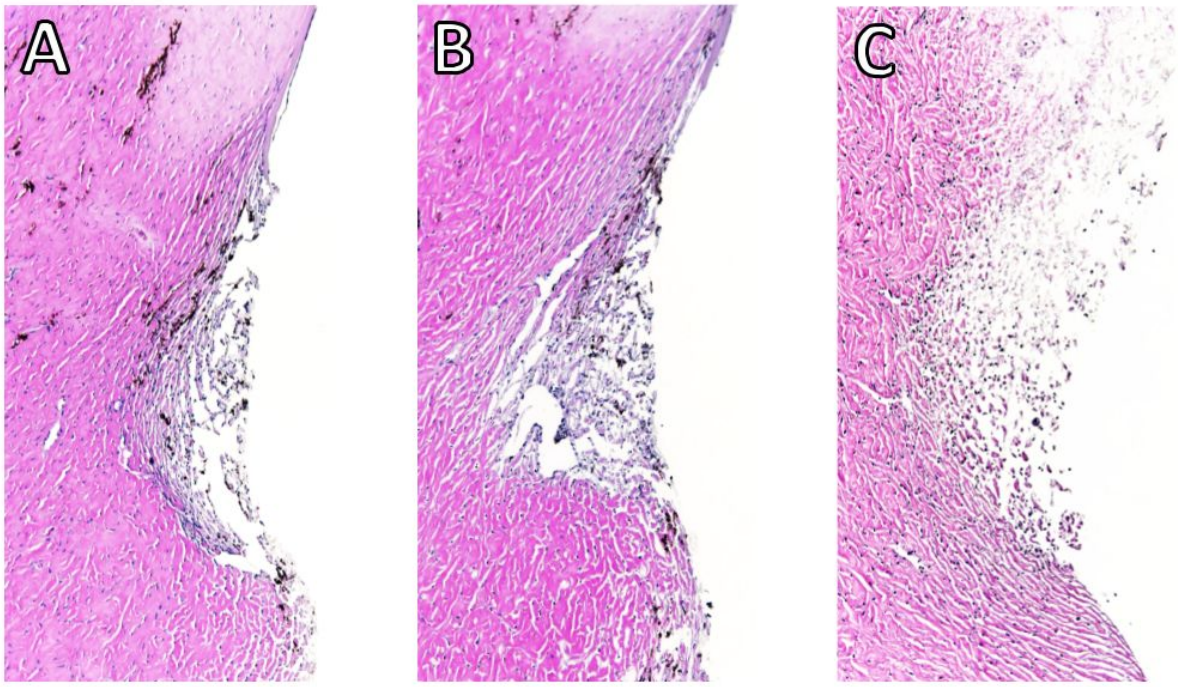

Figure 2. Histology of the angle of perfused anterior chambers. A) Control eyes had a similar appearance to free-thaw treated eyes (B) in early histology slides. C) Saponin treated eyes. Blue nuclei can be seen in all sections at 24 hours.

PeerJ Preprints | https://doi.org/10.7287/peerj.preprints.2736v2 | CC BY 4.0 Open Access | rec: 18 Jan 2017, publ: 18 Jan 2017

Figure 3

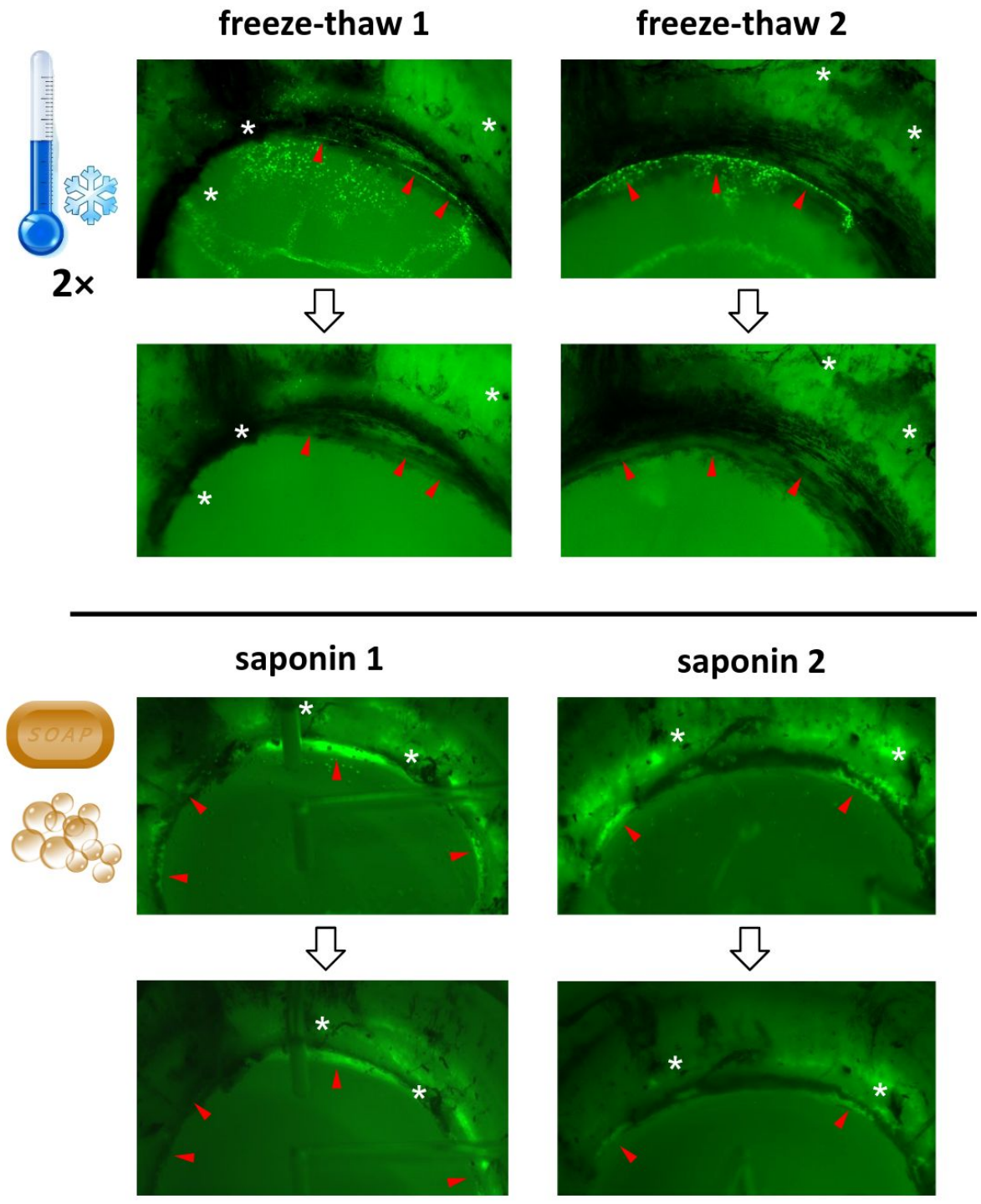

Figure 3: Confirmation of cytoablation. Fluorescence of eGFP expressing, FIV GINSIN transduced cells vanished completely after two freeze thaw cycles (top). In contrast, eGFP can still be seen in many transduced cells but at a reduced intensity in saponin treated eyes (bottom). Red arrowheads point to transduced trabecular meshwork that is ablated completely after freeze thaw but only diminished in saponin eyes. White asterisks indicate landmarks that can easily be recognized before and after treatment.

PeerJ Preprints | https://doi.org/10.7287/peerj.preprints.2736v1 | CC BY 4.0 Open Access | rec: 18 Jan 2017, publ: 18 Jan 2017

Figure 4

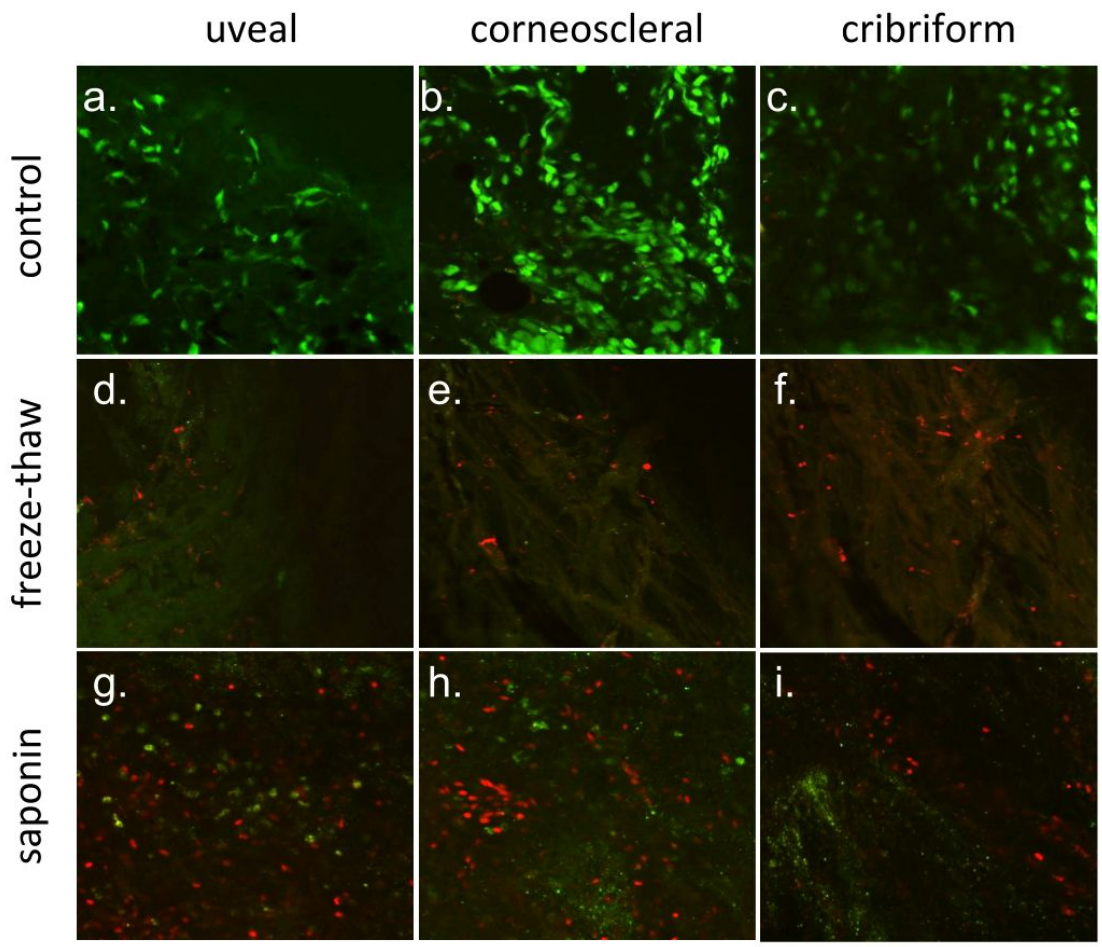

Figure 4. Assessment of TM cell viability by calcein AM/PI co-labelling. Viable trabecular meshwork (TM) cells exposed to calcein AM showed bright green fluorescence, while dead TM cells allowed PI to enter cell membrane and label the cell nuclear with red fluorescence . In the control group, most TM cells were still viable after perfusion for two weeks (a-c). In contrast, cells, including many nuclei, were destroyed by freeze-thaw. No Calcein AM and only a few PI labeled TM cells were found (Figure 5d-Figure 5f). Different from the other two groups, a few TM cells were still alive in the uveal TM and corneoscleral TM (g-h), but most of them were labeled as dead cells by PI.

PeerJ Preprints | https://doi.org/10.7287/peerj.preprints.2736v1 | CC BY 4.0 Open Access | rec: 18 Jan 2017, publ: 18 Jan 2017

Figure 5

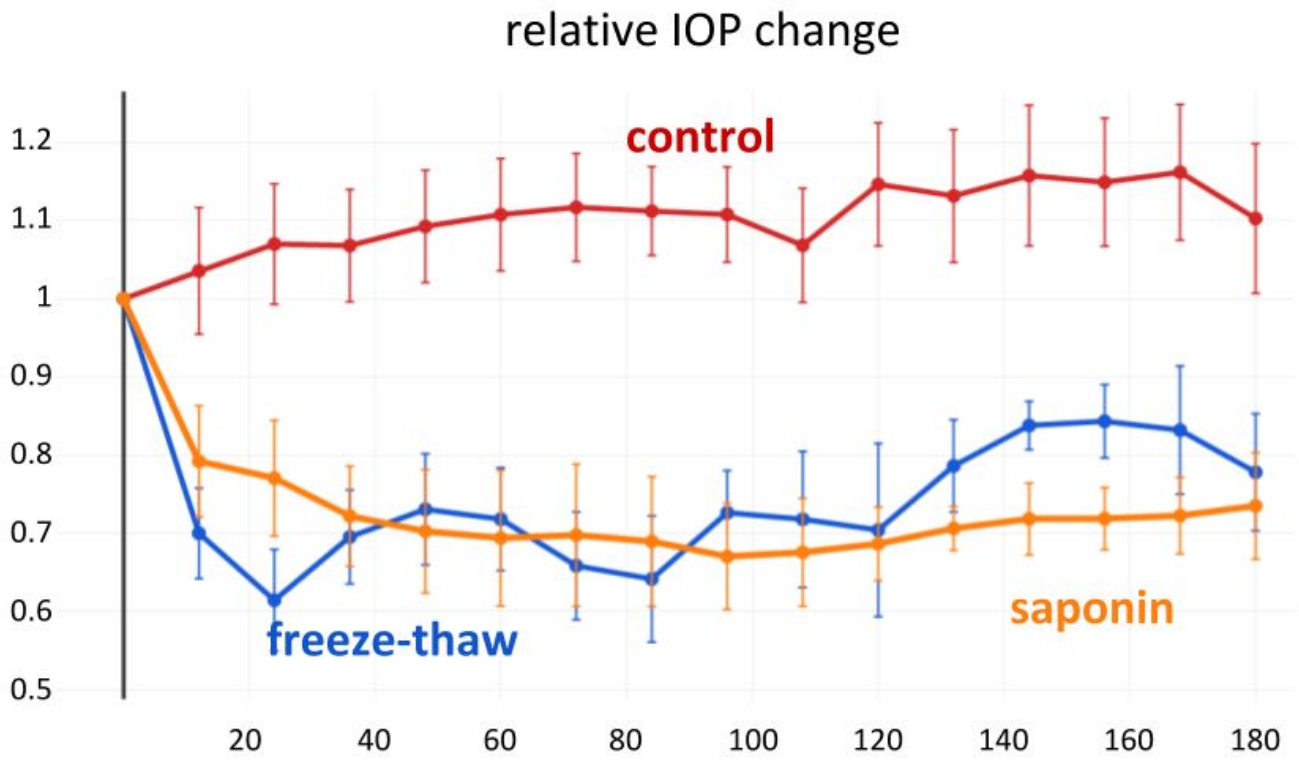

Figure 5. IOP Reduction after TM decellularization. Freeze-thaw (F) resulted in a more rapid IOP reduction than saponin (S) (averages ± SEM). There were no differences at any single time between F and S. Differences between controls and S were not significant onward from 96 hours.

PeerJ Preprints | https://doi.org/10.7287/peerj.preprints.2736v2 | CC BY 4.0 Open Access | rec: 18 Jan 2017, publ: 18 Jan 2017

Figure 6

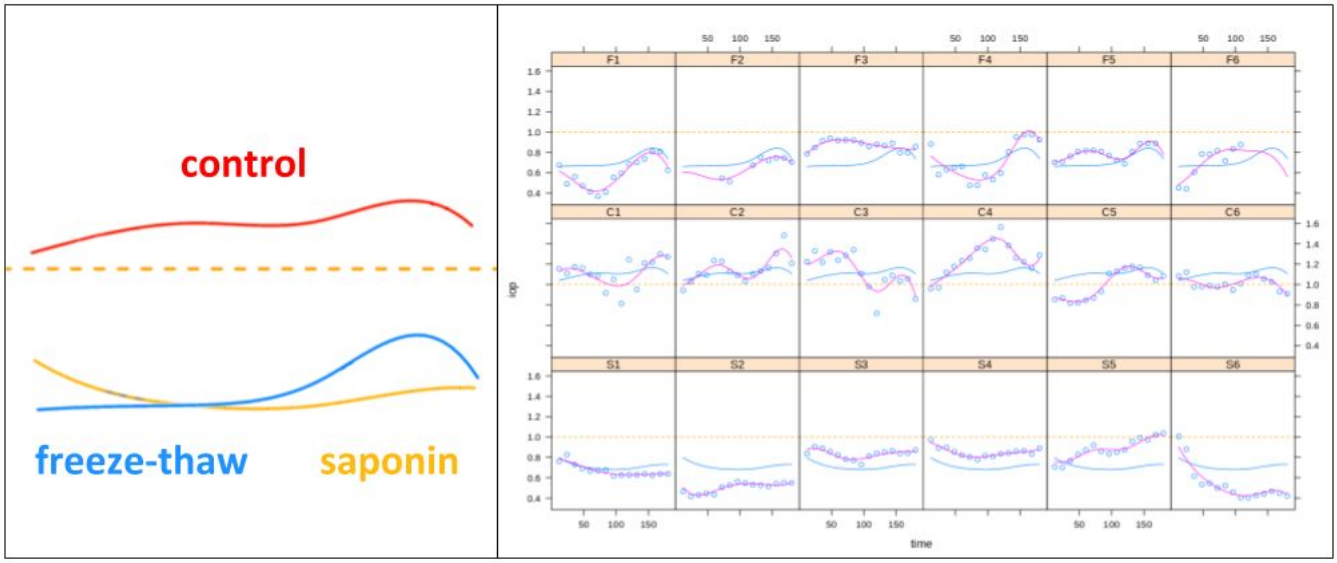

Figure 6: B-spline function of time with 5 degrees of freedom. The b-spline consensus function (left) matched the average IOP changes but allowed to better highlight the response patterns despite a considerable data scatter in the individual curves (right; b-splines shown as blue lines).